EVALUATION OF THE MECHANICAL PROPERTIES OF CAST AND WROUGHT CF8C-PLUS RELEVANT TO ASME CODE CASE QUALIFICATION

Xiang (Frank) Chen, Peter Tortorelli, Michael Santella, Bruce Pint, Hong Wang, Philip Maziasz
Oak Ridge National Laboratory, Oak Ridge, TN, USA

Benjamin Sutton, Daniel Purdy
Electric Power Research Institute, Charlotte, NC, USA

ABSTRACT

The mechanical behavior of a cast form of an advanced austenitic stainless steel, CF8C-Plus, is compared with that of its wrought equivalent in terms of tensile and creep-rupture properties at temperatures up to about 850°C. A traditional Larson-Miller parametric model is used to analyze the creep-rupture data and to predict long-term lifetimes for comparison of the two alloy types. The mechanical behavior of weldments is also assessed. The cast CF8C-Plus exhibited lower yield and tensile strengths but higher creep strength compared to its wrought counterpart. Two welding methods, shielded-metal-arc welding (SMAW) and gas-metal-arc welding (GMAW), met the weld qualification acceptance criteria in ASME BPVC Section IX for the cast CF8C-Plus. However, for the wrought CF8C-Plus, while SMAW and gas-tungsten-arc welding passed the tensile acceptance criteria, they failed the side bend tests due to lack of fusion or weld metal discontinuities. The SMAW cross-weld specimens of cast CF8C-Plus showed higher yield strength but lower tensile strength than the cast base metal. Both SMAW and GMAW cross-weld specimens demonstrated creep rupture strengths generally lower than the average creep strength of the cast base metal, ranging from about 70-110% of the base metal values.

INTRODUCTION

CF8C-Plus initially referred to a cast austenitic stainless steel, officially recognized under the Unified Numbering System (UNS) as J92604 and designated by ASTM as HG10MnN. This advanced alloy represented a significant improvement over its predecessor, CF8C, the composition of which closely matches the wrought type 347 stainless steel [1-3]. Compared to CF8C and type 347 stainless steel, CF8C-Plus exhibits enhanced stability of the desirable austenitic phase, with suppressed formation of delta ferrite and sigma phases. Additional improvement was obtained via the refined distribution of carbides and fine carbonitrides within the alloy's microstructure, resulting in superior high-temperature properties, particularly elevated temperature creep strength. Sufficient mechanical and physical properties data have been accumulated [4, 5] to establish ASME Sec I Power Boilers and B31.1 Power Piping code cases for cast CF8C-Plus [6, 7].

The successful development of cast CF8C-Plus led to an early feasibility assessment to determine if a wrought version of the alloy could be used in high temperature power piping applications [8, 9]. Those studies demonstrated that a wrought austenitic alloy with a matching chemistry to CF8C-Plus could outperform many of the advanced austenitic stainless steels that are used in the design space between ferritic alloys and nickel-based superalloys, some of which are only available in thin-wall tubing and often rely on proprietary thermo-mechanical processing to achieve performance. Further, the wrought version of CF8C-Plus showed mechanical performance comparable to solid solution strengthened Ni-based alloys while the alloy could be produced at a fraction of the cost. For these reasons, efforts have continued to develop and mature a wrought version of CF8C-Plus. These continued efforts have now reached a point where sufficient material data either exist or are currently being collected under existing test programs to consider standardization and code qualification of the alloy for power plant service.

The aims of this paper are to (1) comprehensively assess and compare the tensile and creep properties of both cast and wrought versions of CF8C-Plus, including weldments and (2) qualitatively assess yield strength, tensile strength, and maximum allowable stress values in the context of two approved ASME code cases for cast CF8C-Plus and preliminary analysis for wrought CF8C-Plus.

MATERIALS AND EXPERIMENTAL

Cast CF8C-Plus

Four heats of cast CF8C-Plus with the chemical compositions shown in Table 1 were used in this paper. Each heat was sand cast by Stainless Foundry and Engineering, Inc. (Milwaukee, Wisconsin) into 165mm long, 29mm thick keel bars having a trapezoidal cross section where the two long sides were 22mm and 29mm in width. Specimens from heats 257R, DA20, and T038 were used for the creep-rupture tests while the former two heats and heat T039 were used for tensile testing. Mechanical properties were determined in the as-cast condition.

Table 1: Compositoins of four heats of cast CF8C-Plus.

Heat ID	Cr	Ni	Mn	Nb	Si	Mo	N	Cu	C	P	S	Fe
257R	19.6	12.0	3.7	0.91	0.52	0.37	0.22	0.43	0.09	0.017	0.006	Bal.
T038	19.6	12.4	3.4	0.88	0.59	0.35	0.24	0.36	0.09	0.015	0.004	Bal.
T039	19.1	12.4	3.7	0.96	0.62	0.35	0.23	0.35	0.09	0.025	0.005	Bal.
DA20	19.5	12.6	3.9	0.91	0.45	0.31	0.25	0.49	0.09	0.019	0.006	Bal.

Wrought CF8C-Plus

Four heats have been produced to the CF8C-Plus chemistry and converted to wrought product forms using various processing conditions. The measured chemical compositions from each and wrought conversion processing information are presented in Tables 2 and 3, respectively.

Table 2: Compositions of four heats of wrought CF8C-Plus.

Heat ID	Cr	Ni	Mn	Nb	Si	Mo	N	Cu	C	P	S	Fe
011124	19.48	12.55	3.69	0.95	0.45	0.30	0.26	0.31	0.09	0.032	0.002	Bal.
HF8728	19.61	12.33	4.24	0.82	0.43	0.31	0.26	0.02	0.09	<0.001	0.006	Bal.
HF8726C	19.48	12.27	4.08	0.82	0.41	0.30	0.28	0.02	0.08	0.006	0.005	Bal.
589832	19.68	12.66	3.91	0.75	0.90	0.30	0.26	0.05	0.08	0.014	<0.001	Bal.

Table 3: Wrought CF8C-Plus processing conditions.

Heat ID	Form	Reduction Ratio	Final Heat treatment	ASTM Grain Size
011124 (5:1)	Forging	5:1	1200°C/WQ*	6
011124 (12:1)	Forging	12:1	1200°C/WQ	7
HF8728	Seamless Pipe	9.4:1	1200°C/WQ	7
HF8726C	Seamless Pipe	5.3:1	1200°C/WQ	7
589832	Seamless Pipe	9:1	1170°C/WQ	5.5

*WQ: water quench

The first proof-of-concept heat of wrought CF8C-Plus, 011124, was a 188kg vacuum induction melted ingot that was subsequently hot forged at 1200°C to produce two slabs with thicknesses of 70mm (5:1 reduction) and 32mm (12:1 reduction). The second and third wrought CF8C-Plus heats, HF8728 and HF8726C, were vacuum induction melted ingots weighing 472kg each. The HF8728 and HF8726C ingots were then bored and hot extruded at 1190°C to produce small diameter seamless pipes. Heat HF8728 was hot extruded with a reduction ratio of 9.4:1 to produce a 133mm outside diameter pipe with a 12mm wall thickness. Heat HF8726C was hot extruded with a reduction ratio of 5.3:1 to produce a 152mm outside diameter pipe with a 19mm wall thickness. Additional details regarding the production, initial mechanical testing, and microstructure characterization of Heats 011124, HF8728, and HF8726C have also been reported elsewhere [10, 11].

The production of the newest wrought CF8C-Plus heat, 589832, demonstrated a marked jump in commercial scalability by creating a large heavy wall seamless pipe. Heat 589832 also targeted an optimized chemistry to control Nb-rich precipitate formation during hot working and solution annealing to improve creep performance [12, 13]. Heat 589832 was an electric arc melted ingot weighing over 11,000kg. The 11,000kg ingot was then split and electroslag remelted. A portion from the Heat 589832 remelted ingots was then bored and hot extruded at Wyman-Gordon with a reduction ratio of 9:1 to produce a 406mm outside diameter pipe with a 38mm wall thickness.

The wrought CF8C-Plus materials presented in this paper were solution annealed prior to mechanical testing with the annealing temperature shown in Table 3.

Mechanical Testing

Uniaxial tensile and creep testing were performed to support data package development for eventual ASME Boiler & Pressure Vessel Code qualification of cast and wrought CF8C-Plus. All mechanical testing was performed in accordance with the guidelines presented in ASME BPVC Section II Mandatory Appendix 5. For the measurements of tensile properties, the room temperature and elevated temperature testing was performed per ASTM E8 and ASTM E21, respectively. Creep-rupture testing was conducted per ASTM E139. For ASME Boiler & Pressure Vessel Code qualification, only data from creep-rupture tests with lifetimes > 500h were used in determining the time-dependent stress allowable values. Consequently, in this paper, cast and wrought CF8C-Plus data points with < 500h rupture times were excluded from the analysis. Totals of 59 and 88 datapoints were therefore analyzed for the wrought and cast versions, respectively. In this regard, it should be noted that the results reported here for cast CF8C-Plus are not the same as those presented in a recent paper for the same alloy [5] in which the findings were from creep lifetime analysis for the full dataset, including creep lifetimes < 500h.

Welding

Two full-penetration cast CF8C-Plus welded plates were made to evaluate their properties. One weld was made with the shielded-metal-arc welding (SMAW) process. The base metal for this weld was 50.8mm (2-inch) thick cast CF8C-Plus plates prepared with edge bevels producing a 30° included angle. The set-up included a type 304 stainless steel backing strip allowing the weld to be made entirely from one side in the flat position. Coated, 0.125-inch diameter electrodes conforming to Alloy 117 (SFA-5.11, ENiCrCoMo-1) were used with a total of 80 stringer beads to complete the weld. Interpass temperature was maintained below 149°C (300°F). A second full-penetration weld was made using the gas-metal-arc welding (GMAW) process. In this case, the cast CF8C-Plus plates were 38.1mm (1.5-inch) thick prepared with edge bevels producing a 40° included angle. These plates were set up with a backing strip cut from cast CF8C-Plus. Spooled 0.062-inch diameter welding electrode conforming to Alloy 617 (SFA-5.14, ERNiCrCoMo-1) was used to complete the weldment in the flat position with 18 stringer beads. A 25% He-75% Ar gas mixture supplied at 35 CFH was used to shield the welding arc. Interpass temperature during welding was limited to 177°C (350°F). After welding, tensile and side bend specimens were machined, tested, and evaluated against the weld qualification acceptance criteria presented in ASME BPVC Section IX.

An open root circumferential pipe weldment was created using wrought CF8C-Plus Heat 589832 in a 1G flat position. The weld root and approximately 1/3 of the weld joint were filled with Alloy 617 (SFA-5.14, ERNiCrCoMo-1) via gas-tungsten-arc welding (GTAW). The remainder of the single V-groove was welded with Alloy 117 (SFA-5.11, ENiCrCoMo-1) via SMAW. As with the welded cast CF8C-Plus, tensile and side bend specimens were machined from this weldment and then tested and evaluated against the above-noted ASME weld qualification acceptance criteria.

Creep Lifetime Analysis Based on the Larson-Miller Parameter

The analytical approach used in this paper is based on the well-known Larson-Miller parametric model [14]. In it, the stress function, $f(\sigma)$, is equated to the temperature-compensated Larson-Miller parameter (LMP)

$$f(\sigma) = T(\log t_r + C) \quad (1)$$

where T is the absolute temperature in K, t_r is the time to rupture in hours, and C is a constant. The stress function is expressed as a power series:

$$f(\sigma) = a_0 + \sum a_n (\log \sigma)^n \quad (2)$$

The LMP model is widely used for creep-rupture analysis and most often forms the basis for setting ASME allowable stresses for power boilers and piping under conditions where time-dependent deformation controls an alloy's lifetime. In the analyses that follow, n is set to 3 for the stress function (Eq. 2). This n value yielded the highest correlation coefficient (r^2) without mathematical instability (turnback) over the physically appropriate stress-temperature-time regime for both cast and wrought CF8C-Plus.

To determine the coefficients of the stress function (a_0, a_1, a_2, a_3) and the Larson-Miller constant, C, the Solver function in Excel was used to vary these values to minimize the least squares error between the calculated rupture time as defined by equating Eqs. 1 and 2:

$$t_r = 10\,\hat{}\,(\frac{a_0 + \sum a_n (\log\sigma)^n}{T} - C) \quad (3)$$

and the experimentally determined value at each T and σ. These values for the cast and wrought alloys are shown in Table 4.

Table 4: Optimized Larson-Miller constants and correlation coefficients from regression analyses of CF8C-Plus datasets.

	C	a_0	a_1	a_2	a_3	r^2
Cast	11.7	56720	-52398	23704	-3903	0.58
Wrought	10.6	30863	-20329	9565	-1813	0.63

RESULTS AND DISCUSSION

Tensile

The tensile results from three heats of cast CF8C-Plus are illustrated in Fig. 1. All three heats display comparable yield and tensile strengths, as well as similar strength vs. temperature dependencies over the temperature range of 23-871°C. Heats T038 and T039 exhibit occasional increases in tensile strength, likely attributable to variations in grain size and potential defects in the cast microstructure. Although not depicted in Fig. 1, all three heats demonstrated tensile ductility ranging from 19% to 49%, indicating favorable ductility characteristics.

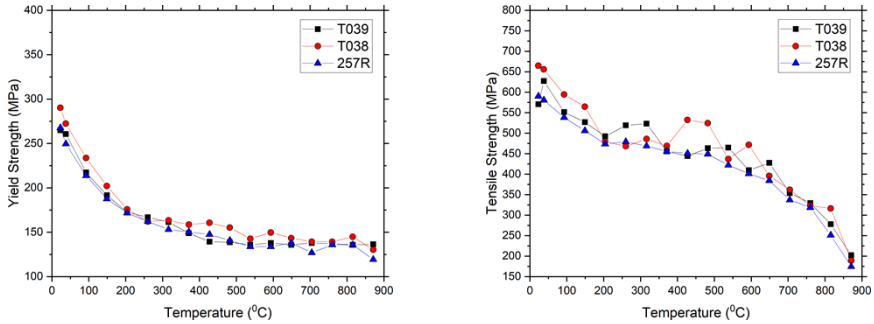

Figure 1: Yield strength in (a) and tensile strength in (b) for three heats of cast CF8C-Plus.

Tensile data collected from the seamless extruded CF8C-Plus pipe heats are presented in Fig. 2. The yield strength of all three heats shows consistent behavior from room temperature to 850°C. Tensile strength trends are also consistent, though heat 589832 exhibits slightly lower strengths than heats HF8728 and HF8726C at temperatures less than 700°C. The lower tensile strength of 589832 is presumably associated with lower Nb concentrations and larger grain size compared to the other two heats. The lower Nb concentration would effectively reduce the equilibrium volume fraction and solvus temperature of potential grain boundary pinning precipitates, allowing for more complete dissolution during hot extrusion and solution annealing which would promote grain growth. The chemistry and grain growth effects are further supported by the fact that there is no clear trend in tensile strength based on the amount of hot work introduced during extrusion and that the final solution treatment temperature of Heat 589832 was actually lower than the other two heats. Regardless of small differences in tensile strength at lower temperatures, heat 589832 tensile data generally exhibit little scatter and agree with previously published results from heats 011124, HF8728, and HF8726C [10, 11]. Though not presented in Fig. 2, all tensile

test results showed reasonable ductility with tensile elongation values greater than 25% across the full test temperature range.

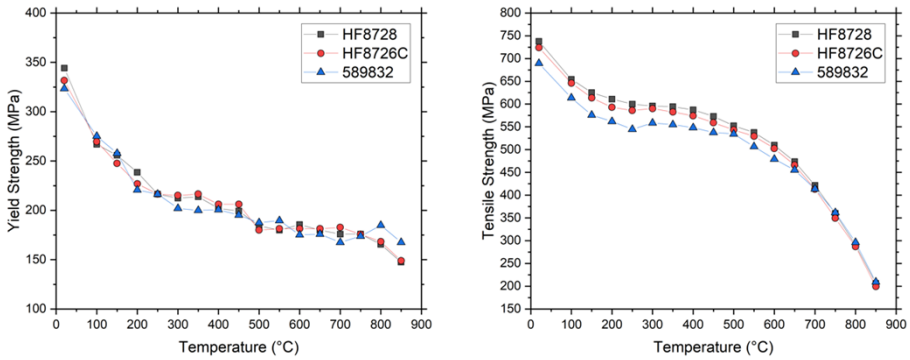

Figure 2: Yield strength in (a) and tensile strength in (b) for three heats of wrought CF8C-Plus.

Based on the tensile results presented in Figs. 1 and 2, it is evident that wrought CF8C-Plus possesses higher yield and tensile strengths compared to cast CF8C-Plus at the same temperatures within the range of 23-850°C. This is expected due to the finer grain size and the wrought microstructure, which are less susceptible to typical casting defects such as porosity.

Creep

The regression analysis results are presented in Fig. 3 for the cast and wrought CF8C-Plus creep database with rupture time > 500h where the curve represents the predicted t_r using the optimized values shown in Table 4. The fitted trend lines describe the cast and wrought creep rupture data relatively well. If a perfect correlation for calculated vs. actual creep rupture lifetimes can be obtained, the slope of a best-fit line on a calculated vs. actual creep rupture lifetimes plot (Fig. 4) should be 1. However, as can be seen in Fig. 4, the data are skewed to the lower side of this line such that the actual slope of the best-fit line is about 0.6 (similar for both cast and wrought dataset). In this case, the predicted values would be conservative.

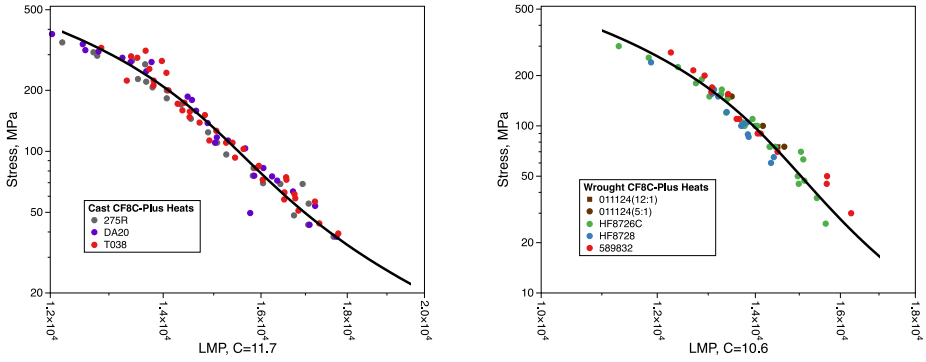

Figure 3: Applied stress vs. LMP for cast and wrought CF8C-Plus in (a) and (b), respectively. Points are experimental data and curves are from regression analysis.

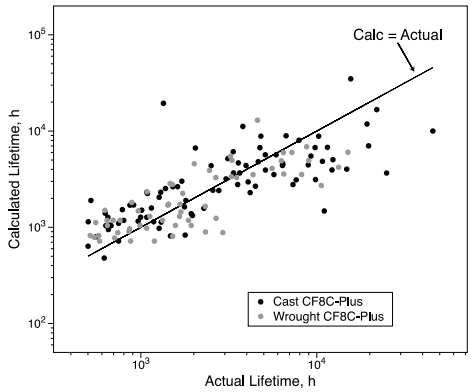

Figure 4: Calculated vs. actual creep rupture lifetimes for cast and wrought CF8C-Plus.

The ability to predict creep lifetimes with some accuracy is obviously critical for extrapolating to times beyond what can be verified experimentally for design purposes (such as when calculating allowable stresses). It is also important when attempting to directly compare materials where respective testing loads and temperatures do not match. This latter situation applies to the present case where the creep-test temperatures for the wrought CF8C-Plus were not the same as those for the cast version. Consequently, for the direct comparison of the creep-rupture resistance of the two CF8C-Plus alloy types, the fitted constants of Table 4 were used with Eq. 3 to calculate creep lifetimes as a function of stress for a series of different temperatures in the range of interest. The results are displayed in Fig. 5a and indicate that the cast CF8C-Plus (dashed curves) has a greater creep resistance than the wrought alloy throughout the temperature range with the difference increasing with decreasing applied stress for the same testing temperature. Supporting this conclusion, Fig. 5b shows the same calculated curves for 600, 650, and 700°C where an approximate comparison can be made with measured rupture times because the differences in test temperatures between the two alloy types were only 7, 1, and 4°C, respectively. Again, the cast CF8C-Plus was stronger than the wrought one in creep testing. While the supporting evidence is not within the scope of this paper, it can be speculated that the greater creep strength of the cast CF8C-Plus is due to its coarse grain size [5] with possible additional strengthening from a fine dendritic substructure.

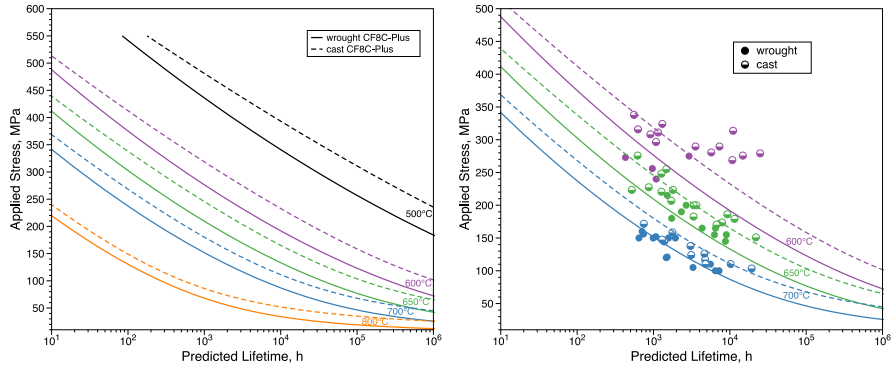

Figure 5: (a) Predicted creep lifetime behaviors for wrought (solid lines) and cast (dashed lines) CF8C-Plus. (b) Measured creep lifetimes for wrought (filled) and cast (half-filled) CF8C-Plus superimposed on predicted lifetime curves where test temperatures of the respective alloys differed by no more than 7°C.

Creep ductility results are presented in Fig. 6 as measured by the elongation to failure as a function of rupture time. Consistent with the findings reported by Purdy and Shingledecker [11], there are two distinct populations observed in creep ductility that are separated around 20-30% elongation. Heats 011124 and 589832 consistently exhibit ductility greater than 30% elongation, while heats HF8728 and HF8726C consistently fall below 20% elongation. The exception to these trends is the few data points from heat 589832 which fall below 20% elongation near 2kh rupture life. A further assessment of these points revealed that these tests were conducted at temperatures between 600-675°C and stresses above 170 MPa. Comparing these test conditions to the elevated temperature tensile test data presented in Fig. 2 shows that the creep loading conditions for these tests exceeded the elevated temperature yield strength of heat 589832.

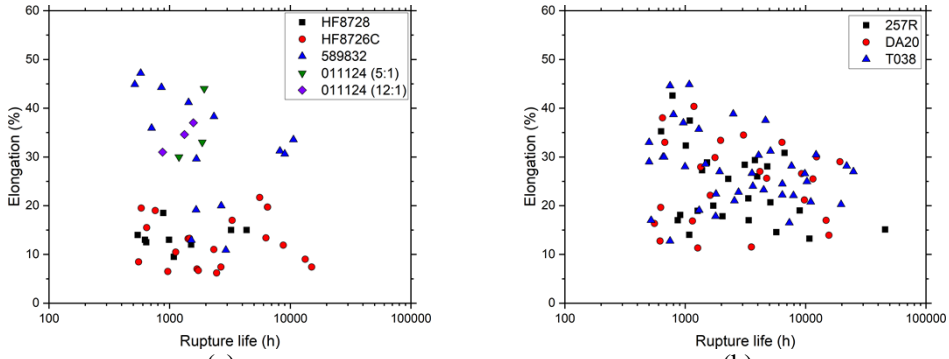

Figure 6: Elongation vs. creep-rupture life for wrought and cast CF8C-Plus in (a) and (b), respectively.

Similar to the wrought CF8C-Plus, the cast alloy version showed an overall large scatter in creep-rupture elongation as shown in Fig. 6b with a weaker tendency for the ductility to decrease with increasing rupture time. However, unlike the former case, each heat displayed a similar scatter band in elongation. The larger spread in creep ductility for the cast CF8C-Plus could be due to the nature of the cast defects in such microstructures.

Weldment Behavior

Details and documentation for cast CF8C-Plus SMAW and GMAW were consistent with ASME Section IX requirements for procedure qualification. Both welds passed the Section IX cross-weld tensile and bend test requirements. Additionally, cross-weld specimens of the SMA weldment were used for tensile testing up to 871°C. Cross-weld specimens from both weldments were used for creep-rupture testing at 593-871°C. The elevated temperature tensile and creep-rupture testing used cylindrical specimens with gage section of 9.53mm (0.375-inch) diameter x 50.8mm (2.0-inch) length. In each cross-weld specimen, the weld deposit was centered in the reduced section gage length.

The variations with test temperature for the yield strength and tensile strength of specimens from the SMAW are shown in Fig. 7 where they are compared to those of the cast CF8C-Plus base metal. All of the cross-weld specimens broke within the cast base metal. For this combination of materials, tensile fractures in the base metal are reasonable because the weld deposit ENiCrCoMo-1 alloy is a version of the Ni-based alloy 617. The tensile properties of alloy 617 are higher than those of cast CF8C-Plus over the test temperature range. Furthermore, the higher yield strength of the cross-weld specimens could have been produced by precipitation reactions (NbN, $Cr_{23}C_6$, Nb_2Cr_2N) in the cast base metal producing a strengthening effect as it was

continually heated during welding. A combination of these same precipitation reactions and strain partitioning between weld metal and base metal could be responsible for the small decrease in tensile strength of the cross-weld specimens. The elongation values of the cross-weld specimens were about half of those for the cast base metal over the entire test temperature range.

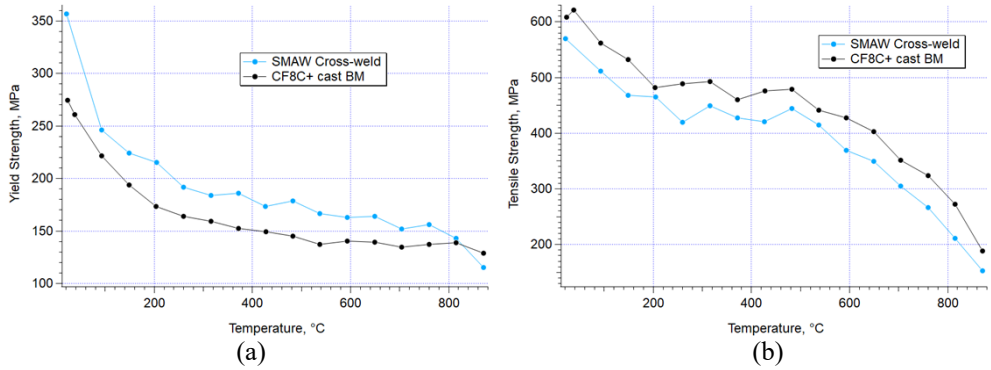

Figure 7: Variation of (a) yield strength and (b) tensile strength with test temperature for cast CF8C-Plus base metal (BM) and cross-weld specimens from an SMA weld.

The cross-weld creep-rupture results from both cast welds are compared to creep results of the cast base metal in Fig. 8 where the variations of applied stress with LMP assuming C=11.7 are plotted. Fig. 8 suggests that the creep-rupture strengths of the cross-weld specimens are generally within the scatter of the base metal. A clearer comparison is between cross-weld rupture stress and base metal creep stress at fixed LMP shown in Fig. 9. For this comparison, a 3rd-order polynomial fit through the base metal results, shown as the dotted line in Fig. 8, was used to define base metal values for the Fig. 9 comparison. Figure 9 indicates that the cross-weld rupture strengths are generally lower than the average creep strength of the cast base metal, ranging from about 60-120% of base metal values at fixed LMP. In addition, the creep ductility of cross-weld specimens ranged from 4% to 19%, which is about half of the base metal creep ductility depicted in Fig. 6b.

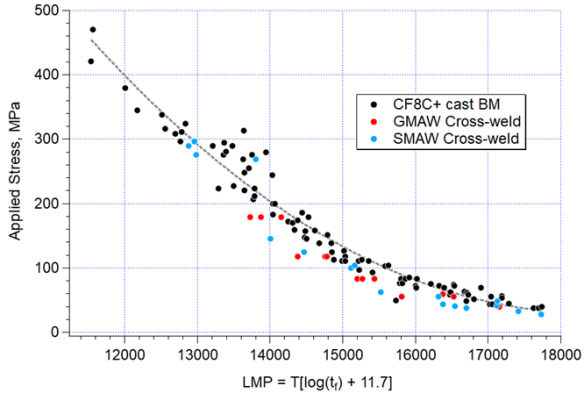

Figure 8: Variation of stress applied during creep-rupture testing with Larson-Miller parameter for both cast CF8C+ base metal, and cross-weld specimens from both the SMAW and the GMAW. The dotted line represents and 3rd-order polynomial fit through the base metal results.

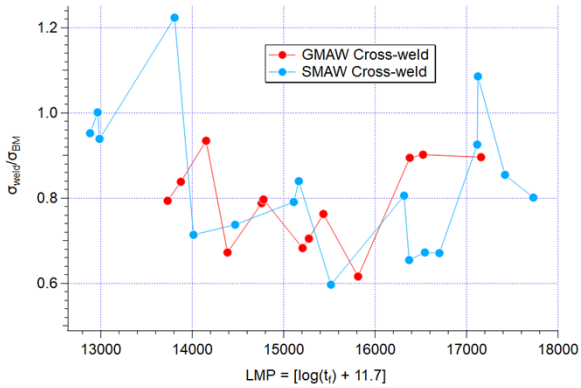

Figure 9: Variation of the ratio of cross-weld rupture stress σ_{weld} to average base metal creep stress σ_{BM} with Larson-Miller parameter for both cast welds.

Four side bend specimens from the wrought CF8C-Plus weldment failed to meet ASME Section IX acceptance criteria. Two samples failed due to lack-of-fusion at the weld root, and two samples failed due to discontinuities in the weld metal. These failures do not necessarily indicate a lack of weldability but do mean that further welding and mechanical testing work are needed to generate weldments that meet the bending criteria and produce cross-weld tensile and creep rupture data to establish weld strength reduction factors for wrought CF8C-Plus. Nevertheless, despite this lack of weld quality, two cross-weld tensile samples were tested at room temperature from each weld metal region of the wrought CF8C-Plus weldment. Both Alloy 617 cross-weld tensile samples failed in a ductile fashion within the base metal with an ultimate strength of approximately 670 MPa. Both Alloy 117 cross-weld tensile samples failed in a ductile fashion, however one sample failed in the weld metal with an ultimate strength of 672 MPa and one sample failed in the base metal with an ultimate strength of 689 MPa.

CONCLUSIONS

CF8C-Plus is a promising structural material, offering enhanced stability of the desirable austenitic phase and superior high-temperature properties due to a refined distribution of carbides and fine carbonitrides within the alloy's microstructure. The cast version of this steel has obtained ASME code case approval for Section I Power Boilers and B31.1 Power Piping, while the wrought version is currently accumulating qualification data for a near-future Section I code case application. This paper comprehensively assesses and compares the tensile and creep properties of both cast and wrought versions of CF8C-Plus, including their weldments, using datasets that meet code case criteria.

It was found that the cast CF8C-Plus exhibited lower yield and tensile strengths but higher creep strength compared to its wrought counterpart. Two welding methods, SMAW and GMAW, met the weld qualification acceptance criteria in ASME BPVC Section IX for the cast CF8C-Plus. However, for the wrought CF8C-Plus, while SMAW and gas-tungsten-arc weldments showed acceptable tensile strength, they failed the side bend tests due to lack of fusion or weld metal discontinuities. The SMAW cross-weld specimens of cast CF8C-Plus showed higher yield strength but lower tensile strength than the cast base metal. Both SMAW and GMAW cross-weld specimens of the cast CF8C-Plus demonstrated creep rupture strengths generally lower than the average creep strength of the cast base metal, ranging from about 70-110% of the base metal values.

ACKNOWLEDGMENTS

This project is sponsored by the U.S. Department of Energy, Office of Fossil Energy and Carbon Management, with Award Number FWP-FEAA133 under contract DE-AC05-00OR22725 with Oak Ridge National Laboratory (ORNL) managed by UT Battelle, LLC. We are grateful to J. Hissam from National Energy Technology Laboratory for the programmatic support. We also would like to thank J. Moser, S. Hawkins, K. Epps, D. Kyle, and D. Stringfield from ORNL for their technical support and S. Bailey from Electric Power Research Institute for the welding support.

REFERENCES

[1] Shingledecker, J.P., et al., *CF8C plus: a new high temperature austenitic casting alloy for advanced power systems.* Energy materials, 2006. **1**(1): p. 25-32.
[2] Shingledecker, J.P., et al., *Creep behavior of a new cast austenitic alloy.* International journal of pressure vessels and piping, 2007. **84**(1-2): p. 21-28.
[3] Chen, X. and E. Lara-Curzio, *Reanalysis of Cost and Moist Air Oxidation Performance for CF8C-Plus and Other Alloys for AUSC Applications*. 2021, https://doi.org/10.2172/1782110.
[4] Pint, B.A., *Deployment of CF8C-Plus Cast Stainless Steels*. 2013, https://doi.org/10.2172/1097486
[5] Santella, M.L., et al., *Predicting the creep-rupture lifetime of a cast austenitic stainless steel using Larson-Miller and Wilshire parametric approaches.* International Journal of Pressure Vessels and Piping, 2023. **205**: p. 105006.
[6] *2023 ASME Boiler and Pressure Vessel Code Supplement 4, Section I Case 3049-1*, *ASTM A351/A351M-14 Grade HG10MnN (UNS J92604)*, 2024.
[7] *ASME B31 Code Case for Pressure Piping, B31.1 Case 199-2*, *ASTM A351 Grade HG10MnN, UNS J92604*, 2023.
[8] EPRI, *Program on Technology Innovation: A Wrought Advanced Creep-Resistant Austenitic Stainless Steel for High Temperature Fossil Power Plant Applications – A Feasibility Assessment*. 2010, Palo Alto, CA, 1021249
[9] Gandy, D., et al., *Mechanical properties and microstructure of a wrought austenitic stainless steel for advanced fossil power plant applications.* Advances in Materials Technology for Fossil Power Plants - Proceedings from the 6th International Conference, 2011: p. 916-932.
[10] EPRI, *Wrought Advanced Creep-Resistant Austenitic Stainless Steel for High-Temperature Fossil Power Plant Applications: A Feasibility Assessment*. 2013, Palo Alto, CA, 3002001711
[11] Purdy, D., D. Gandy, and J. Shingledecker, *Characterization of an extruded austenitic stainless steel for advanced fossil power plant applications.* Advances in Materials Technology for Fossil Power Plants - Proceedings from the 7th International Conference, 2014: p. 1059-1070.
[12] Purdy, D., et al., *Microstructure Impacts on Mechanical Properties in a High Temperature Austenitic Stainless Steel*. 2017. p. 1288.
[13] EPRI, *Manufacturing Studies of a High-Temperature Stainless Steel*. 2017, Palo Alto, CA, 3002009212
[14] Larson, F.R. and J. Miller, *A time-temperature relationship for rupture and creep stresses.* Trans. ASME, 1952. **74**: p. 765-775.